Scientific Research Publishing

International Journal of Geosciences, 2022, 13, 951-972
https://www.scirp.org/journal/ijg
ISSN Online: 2156-8367
ISSN Print: 2156-8359

Simplifying the Integration of Petrophysics and Rock-Physics to Identify Hydrocarbon Bearing Rocks on Seismic

Arfan Ali, Erick Alvarez

Shell UK Limited, Aberdeen, UK
Email: arfan.ali@shell.com

How to cite this paper: Ali, A. and Alvarez, E. (2022) Simplifying the Integration of Petrophysics and Rock-Physics to Identify Hydrocarbon Bearing Rocks on Seismic. *International Journal of Geosciences*, **13**, 951-972.
https://doi.org/10.4236/ijg.2022.1310048

Received: September 19, 2022
Accepted: October 28, 2022
Published: October 31, 2022

Abstract

A considerable effort has been made in the literature for quality assurance (QA) and quality checking (QC) of the petrophysical log data for computation of reservoir rock property parameters. Well log data plays an integral role in building a rock physics model for quantitative interpretation (QI) work. A poor-quality rock physics model may lead to significant financial and HSSE implications by drilling wells in undesired locations. Historically, a variety of techniques have been used including histograms and cross plots for reviewing the feasibility of petrophysical logs for QI work. However, no attempt has ever been made to introduce a simplified workflow. This paper serves two-fold. It provides a simplified step by step approach for building a petrophysics/rock physics model. A case study has been presented to compare the synthetic seismogram generated from the simplified workflow with the actual seismic trace at well locations. Secondly, the paper shows how a few key cross plots and rock property parameters provide adequate information to validate petrophysical data, distinguish overburden and reservoir sections, and to help identify fluids and saturation trends within the reservoir sands. In the mentioned case study, the robustness of the simplified rock physics model has helped seismic data to successfully distinguish hydrocarbon bearing reservoir sands from non-reservoir shales.

Keywords

Petrophysics-Rock Physics Integration, Rock Physics Model, Quantitative Interpretation, Simplified Workflow, Seismic to Well Tie

1. Introduction

Historically, a lot of effort has been made to utilize seismic amplitudes, seismic

inversion and quantitative interpretation (QI) techniques in the hydrocarbon industry [1] [2]. Seismic inversion techniques have been considered for informing shallow geological site investigations [3]. Work by Domenico [4] concluded that estimation of gas concentration from seismic amplitude data alone is not possible due to a non-linear relationship between compressional velocity (V_p) and gas concentration. Castagna and Greenburg [5] [6] provided relationships between compressional (V_p) and shear velocities (V_s) in clastic rocks. They also mentioned the significance of empirically derived relationships in the absence of in situ measurement of V_p, V_s, and density values. The Gardner equation [7] allowed estimation of V_p from density or *vice versa*. Faust [8] along with Kim-Rudman [9] and Smith's equation [10] described the relationship between resistivity and V_p. Zoeppritz [11] described behaviours of reflected and refracted signals for both compressional wave (P-wave) and shear wave (S-wave) for a variety of elastic parameters. The subsequent simplifications were proposed by Aki and Richards [12], and Shuey [13]. One of the most important relationships between V_p, V_s, density, lithology, and pore fluid fill was proposed by Gassmann [14], and Geertsma and Smit [15].

In the past decade or so, the integration of petrophysics and seismic data has been revolutionary in the hydrocarbon industry for drilling exploration, appraisal, and development wells [16] [17] [18]. The time lapse improvements in data acquisition, processing, and analysis has provided significant help in optimized target locations both in the overburden (OB) and reservoir sections [8] [19].

The petrophysical data plays a key role in any rock physics model and seismic inversion work. Without appropriate data conditioning, a good prospect can easily be made like a "no prospect" and vice versa. The published literature, however, has given little emphasis in providing a simplified workflow for petrophysics/rock physics model. It is primarily down to the fact that the vast majority of seismic professionals tend to incline towards geophysics expertise. This potentially leads to a gap in the literature in understanding the importance of petrophysical data conditioning. The present work has therefore made an attempt to fill this gap. It is shown in the paper that a few key steps play a tremendously important role to ensure the robustness of log data quality before feeding into the rock physics model.

2. Petrophysics-Rock Physics Integration—A Simplified Workflow

A good quality log data forms the backbone of any rock physics model. This paper shows how a few key cross plots can be used to provide sufficient confidence in the robustness of the log data for building a rock physics model. A step-by-step approach of the simplified workflow is shown in **Figure 1**. It consists of the following key elements:

- Log data conditioning using key histograms and cross plots (step 1).

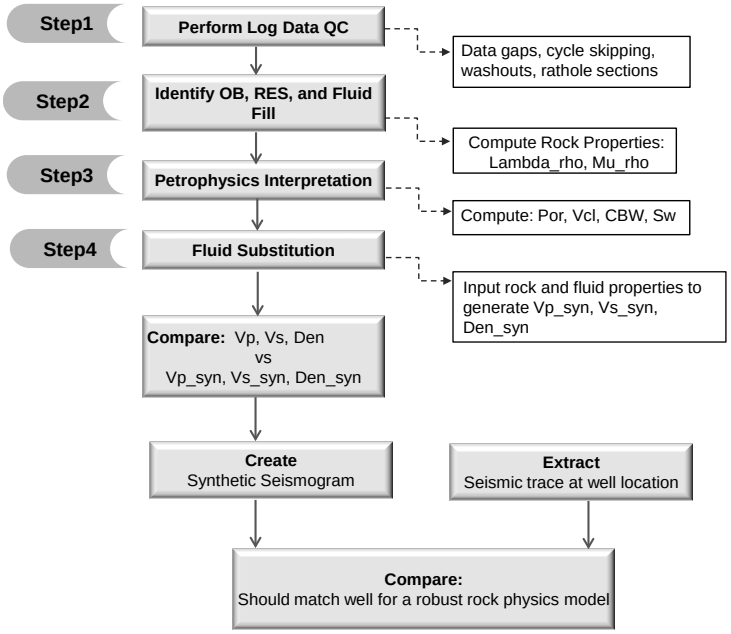

Figure 1. Simplified workflow for building a rock physics model.

- Computation of rock properties to identify reservoir and overburden intervals, and fluids (step 2).
- Computational of petrophysical parameters to input into the rock physics model (steps 3, 4).
- The above is incorporated in the comparison of synthetic seismograms with seismic trace at well locations, and for subsequent seismic inversion.

Petrophysical log data including bulk density (DEN), compressional velocity (V_p), and shear velocity (V_s) are used to compute both rock property parameters Lambda_rho ($\lambda_{\_rho}$) and Mu_rho ($\mu_{\_rho}$), and petrophysical parameters including porosity (Por), volume of clay (Vclay), clay bound water (CBW), and water saturation (Sw). The rock property parameters are used to identify between the overburden and reservoir sections. The petrophysical parameters and the bulk moduli of minerals and fluids (discussed later in the paper) are used in the fluid substitution for generating synthetic compressional velocity (V_p_syn) and synthetic shear velocity (V_s_syn). The synthetic logs are then used in generating synthetic seismogram which when compared with the actual seismic trace can help interpret horizons at well locations. This is shown by a workflow in Figure 1. Synthetic seismograms essentially provide a calibration point for the actual seismic trace at the well location. For instance, if there is a hard kick on seismic, synthetic seismogram basically confirms that this is due to a hydrocarbon bearing reservoir. Once the seismic data is calibrated at well locations, this can be extended away from the wellbore to understand the structure (formation horizons) and lateral extent of the reservoirs including pinch outs. In case of multiple wells in the area, one can correlate horizons and reservoir intervals between the wells. The rest of the paper elaborates on the individual steps in Figure 1 for a simplified petrophysics/rock physics integration.

2.1. Step-1: Log Data QC

Log data QC is the most crucial step as the subsequent petrophysical (PP) interpretation and the quality and reliability of the entire rock physics model is dependent on the input log data. Poor quality logs and inadequate PP interpretation can make an attractive prospect look unattractive/uneconomical on seismic derived rock properties. A good practice is to always show the available log data from the contractor in the form of Table 1. The data quality remarks from the contractor can be shown in the form of flags (red, green and amber) in order to immediately understand the quality of the log data prior to any QC. This is shown in Table 2. This helps to understand the amount of available log data which is of good quality, and to exclude wells with poor quality data at an early stage. This also provides a high-level view of the amount of time and resources required for log data QC.

The preliminary log data QC includes depth shifting of log data in individual hole sections followed by joining log data for different hole sections. A poor depth shifting will impact the acoustic impedance (AI) log which is a product of bulk density (DEN) and compressional transit time (DT). This will subsequently impact on the quality of synthetic seismogram and seismic to well tie. Figure 2(a) shows an example where one would need to correct for depth shifting (density and sonic logs are off depth in this case).

In addition to depth shifting, the Vp and Vs logs are analysed for cycle skipping effects. Cycle skipping is the occurrence of a failure to detect first arrival of the sonic wave. This causes a marked and sudden shift to higher DT. If not corrected, this can cause an anomaly on the AI response and synthetic seismogram which one can misinterpret for a geological horizon. Therefore, it is absolutely essential for the log data to be edited and repaired, if required, for cycle skipping. Figure 2(b) shows an example where one would need to correct for cycle skipping.

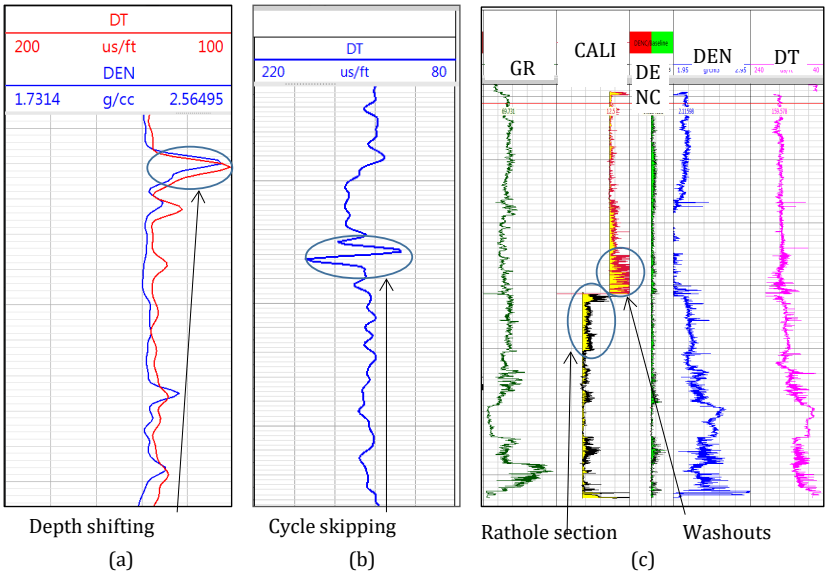

Figure 2. (a) Log data issue with depth shifting; (b) Effect of cycle skipping on acoustic log; (c) Washout intervals above and below the casing shoe.

Table 1. Available log data and calculated petrophysical properties. See the "abbreviations" section for acronym definitions.

		Available log data						Calculated Rock Properties				
WL/LWD	**Mud**	**CALI**	**DEN**	**DT**	**GR**	**NEU**	**RESD**	**VSH**	**POR**	**PERM**	**SW**	**BVW**
WL	WBM	X	X	X	X		X LL7	X GR	X D	X	X AR	X
MWD	OBM				X			X GR	X D	X	X AR	X
WL	OBM	X	X	X	X	X	X RILD	X ND	X D	X	X AR	X
WL	WBM	X	X	X	X	X		X ND	X D	X	X AR	X
WL	OBM	X	X	X	X	X	X RILD	X ND	X D	X	X AR	X
WL	WBM	X	X	X	X	X	X RD	X GR	X D	X	X AR	X

Table 2. Log data QC and quality flags.

Well name	Log Data Quality	Comments
1	**Poor**	Data gaps in 12.25" hole due to sensor failure
2	**Poor**	Significant washouts in "C" Formation.
3	**Fair**	Washouts inside the rathole section and below the casing shoe.
4	**Fair**	Washouts within "B" Formation.
5	**Good**	Data is available across the entire section of interest.
6	**Good**	A small data gap in 12.25" hole due to sensor offsets

The log data also requires editing and patching across washout intervals, rathole sections, and for data acquired inside the casing. The depth of investigation of majority of the logging tools is not very deep. The log data is therefore compromised across washout intervals. Shales have a tendency to swell and washed away especially in wells where water-based mud (WBM) is used during drilling. Washout sections are also often seen below the casing shoe (rathole section) where log data is compromised due to the presence of cement. Figure 2(c) shows an example of washout intervals inside the rathole section below the casing shoe, and in the overburden above the casing shoe. The respective intervals are obvious on the clipper log shown by the circles in the overburden and rathole sections.

Another useful way of identifying poor quality log data is to plot the log data versus depth. Figure 3(a) shows the DEN log (y-axis) plotted against depth (x-axis). The data has been color coded with the density correction log (DRHO). The anomalous data points are highlighted in brown. In Figure 3(b), the DRHO log (track 2 from right) and the photoelectric factor log (PEF—track 3 from right) show anomalous response across the highlighted interval. The higher values of the DRHO are indicative that a correction is required to the DEN log data. The PEF data responds to molecular weights of the formation minerals. In case of washouts, it is the enlarged borehole the tool looks into and therefore shows anomalous data. In short, the various log data support each other to correct for DEN log in the highlighted interval (data patching techniques will be discussed later in this paper).

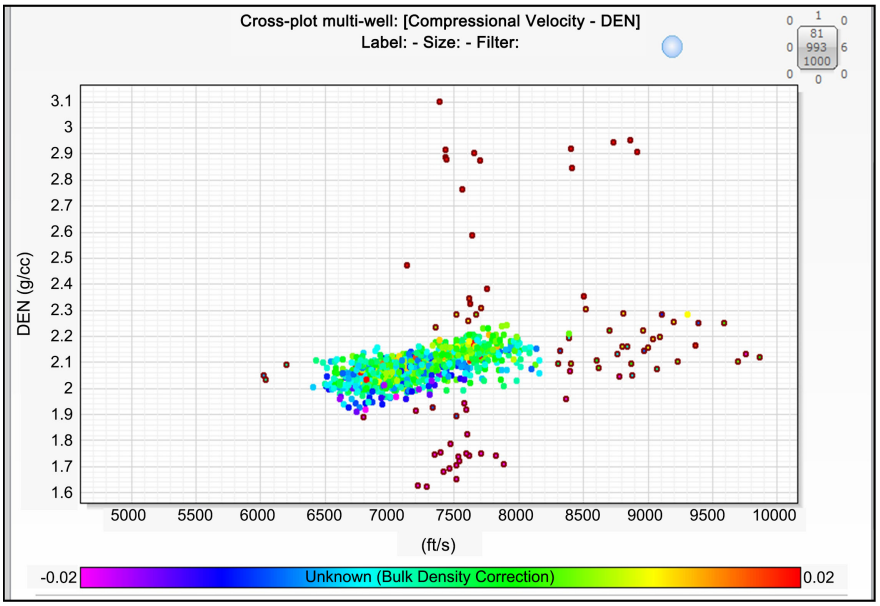

(a)

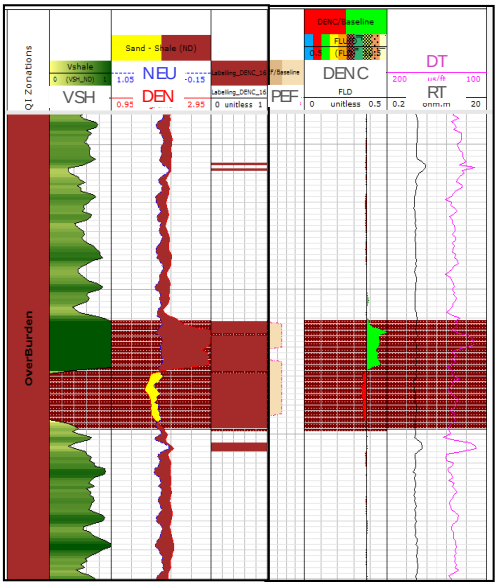

(b)

Figure 3. (a) Crossplot of bulk density log (y-axis) versus depth. The anomalous data points are highlighted in "brown"; (b) Log plot showing shale volume from neutron and density logs (track 6 from right), neutron-density logs (track 5), PEF (track 3) and DRHO (track 2).

An important point to note here is that it is not always the case that spurious log data would need to be removed from the logs. **Figure 4(a)** shows DEN log (x-axis) plotted against depth (y-axis). The anomalous data points on the crossplot in **Figure 4(a)** are highlighted in brown. **Figure 4(b)** shows NEU and DEN logs (track 1 from right), and GR log (track 2 from right). The anomalous data points on the right-hand side of the DEN trend in **Figure 4(a)** belong to the calcite stringer (evident by low GR and high DEN values in **Figure 4(b)**). The points to

the left hand side of the crossplot in Figure 4(a) belong to a thin sand (evident by low GR and ND crossover in Figure 4(b)). It is now obvious that the anomalous data is real in this case and reflects the formation rock signatures and therefore should not be removed from the log data. In fact, the calcite stringers could provide a suitable calibration point for correlation on seismic. If such anomalous data is removed from the logs, the anomalies due to calcite stringers would disappear in the rock physics model and one may see inconsistencies between the rock physics model and seismic data which would merely be due to the poorly conditioned log data.

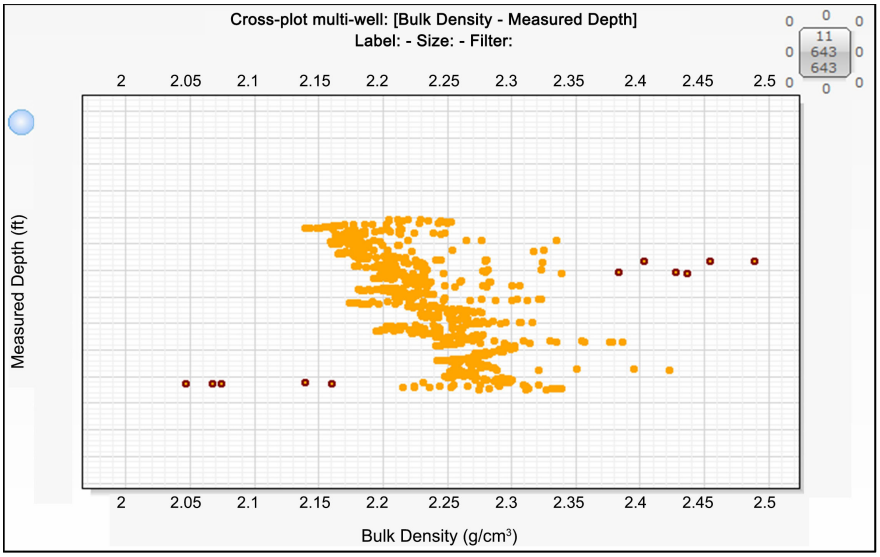

(a)

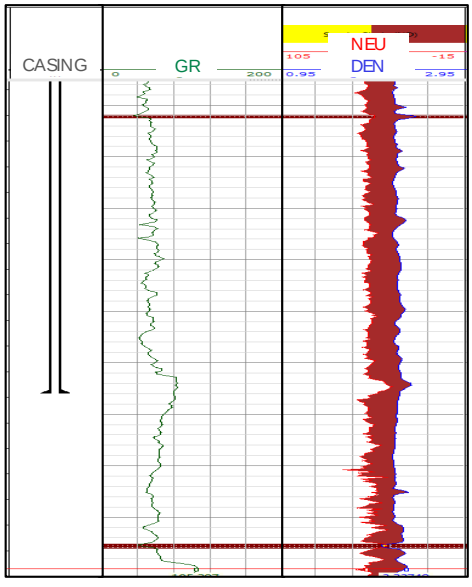

(b)

Figure 4. (a) Crossplot of bulk density log versus depth (y-axis). The anomalous data points are highlighted in "brown"; (b) The neutron and density log data (track 1 from right) and gamma ray log (track 2). The highlighted log data is shown in "brown".

Often both DEN and Vp logs show an increasing trend with depth. This is due to an increase in the overburden mass of the rock with depth. Although the overall trend of the DEN log in Figure 4(a) shows an increase in the bulk density with depth, localized density trends are also observed with depth. This is due to a change in the density of individual formations as the tool goes through different rock layers. This is essentially the reason why one sees different horizons on the seismic amplitude map.

So far the paper has looked at identifying and conditioning the anomalous log data. In addition to log conditioning, there are a few key cross plots which one can use to understand quality of the log data. In Figure 5(a), the DEN log (y-axis) of the underburden formation is plotted against V_p (x-axis). Figure 5(b) shows a similar crossplot for the overburden. The crossplots are color coded with "caliper minus bitsize" scaled from 0 - 4 inches. On the color code bar, anything above 0 would mean an enlarged hole size and anything below zero would mean mud cake build up on the borehole walls. Such color coding immediately allows one to highlight intervals for an undergauge or overgauge hole. For instance, in Figure 5(b), the overburden section is heavily washed out whereas the underburden section (Figure 5(a)) shows the hole still in good shape with diameter close to the bit size. This immediately shows that the data quality in the overburden section may have been compromised due to the washouts.

There are instances where one might see multiple data trends in the over/underburden and which may reflect the real stratigraphy of the formation. In Figure 6(a), there is a kick in the DT (track 1 from right), DEN (track 2 from right), and GR logs (track 5 from right) midway into the overburden. This is shown by shaded vs non-shaded interval of the log plot. The log data has been acquired as part of the same logging run. The fact that each of the tools on the toolstring show a kick at this depth, this emphasizes on the data validity and true response of the formation. Figure 6(b) shows a crossplot of DEN (x-axis) versus DT (y-axis) which clearly shows the two trends.

Another useful crossplot for supporting (or otherwise) the validity of the two trends is to plot DEN (y-axis) against Vsh (x-axis) and color code with GR. This is shown in Figure 6(c). In this crossplot, for a given Vsh, the lower GR values would correspond to lower density values. This is typical as silty shales have lower densities and lower gamma ray values, whereas clay rich shales have higher densities and higher gamma ray values (red points). The crossplot in Figure 6(c) confirms the presence of two separate shale packages in the overburden each starting with high silt content (low gamma ray, low shale volume and low density values) to a low silt content (high gamma ray, high shale volume and high density values). One however needs to check this information against geological information (for example, changes in the depositional environment), analogue wells in the area, and cutting descriptions.

It is often the case that wells used for the rock physics model have been drilled/

logged in different times using different contractors and with different logging tools. If there was a systematic shift in the log data in certain wells (for example due to calibration errors on the logging tools), this would cause a shift in the acoustic impedance response among the wells under study. Figure 7 shows a histogram of Vp across six wells. The compressional velocity in the well in "pink" shows an offset. One needs to understand if this response is real and represents the geology of the area or if this is due to a systematic error. If later, one would be underestimating acoustic impedance and which would translate into the synthetic seismograms as part of the rock physics model.

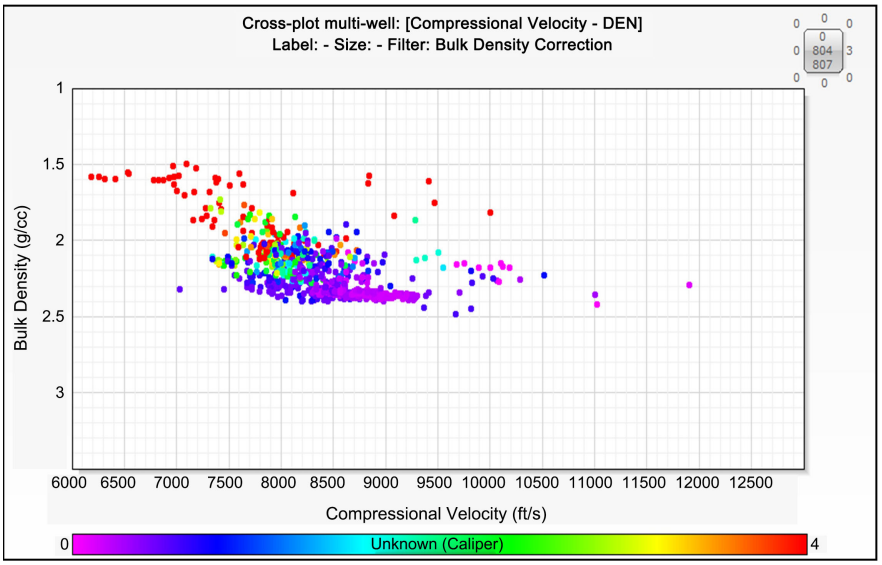

(a)

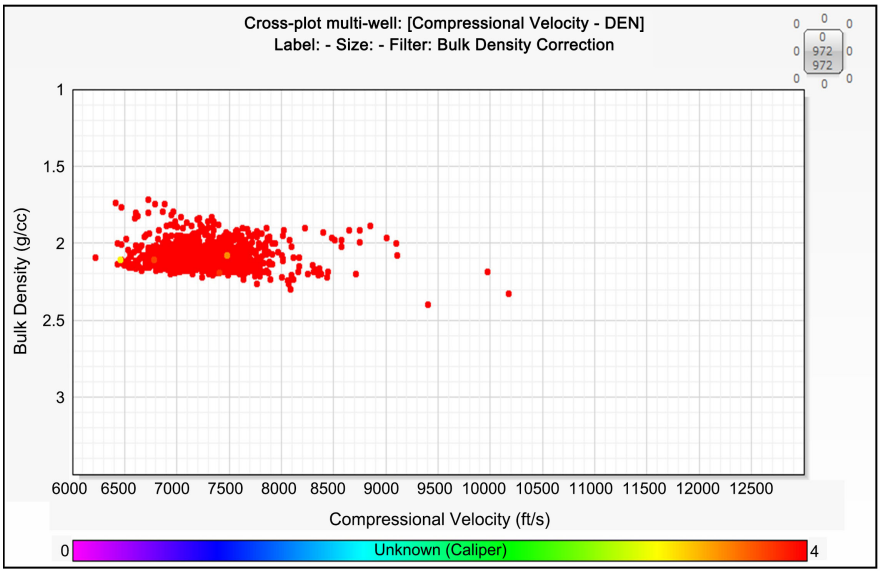

(b)

Figure 5. (a) Crossplot of compressional velocity versus bulk density log (y-axis) for the underburden, color coded with "caliper minus bitsize"; (b) The same crossplot for the overburden.

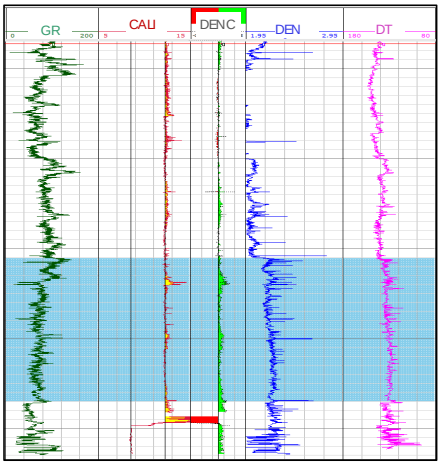

(a)

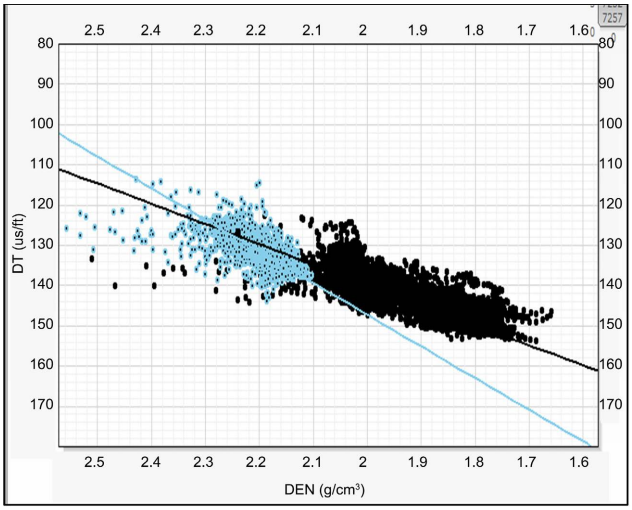

(b)

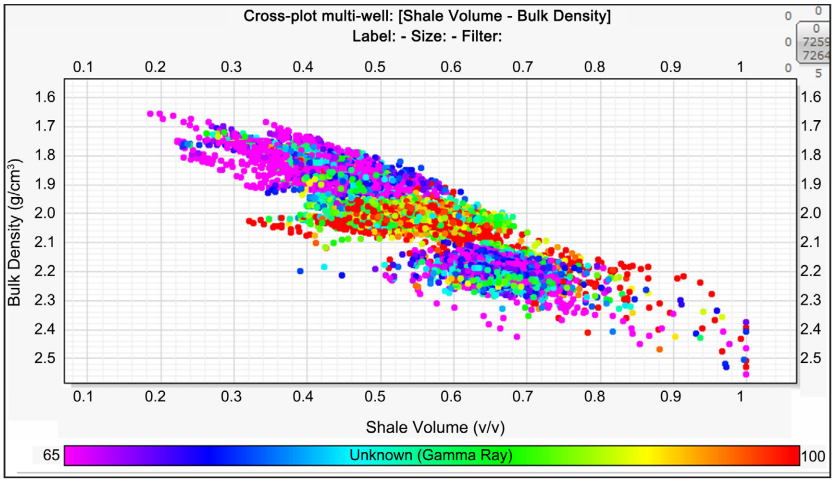

(c)

Figure 6. (a) Log data showing a kick midway through the overburden formation; (b) Crossplot of density versus transit time showing the two trends within the overburden formation; (c) Crossplot of bulk density against shale volume and color coded with gamma ray.

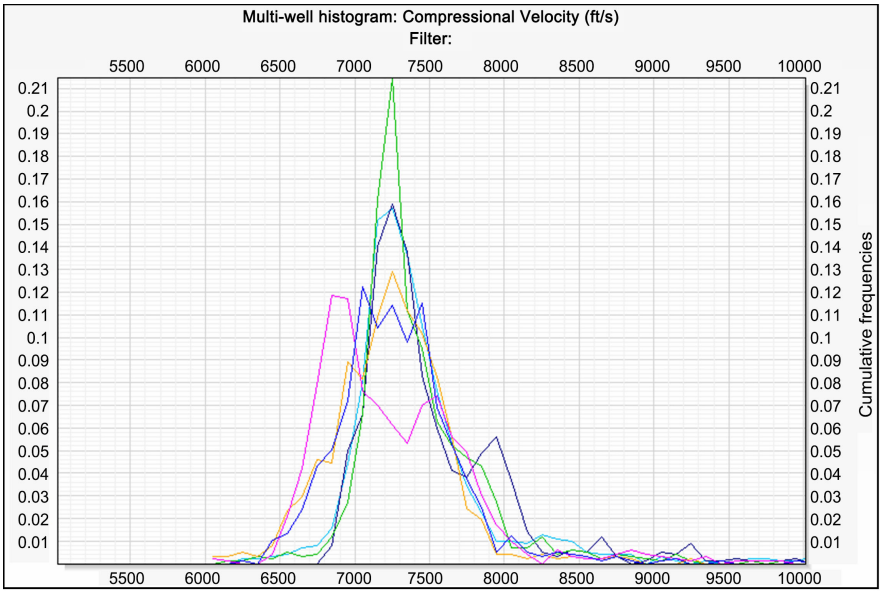

Figure 7. Multiwell histogram of density log data for wells under study.

One of the important steps in log data QC is to create synthetic logs in order to patch sections with missing log data (due to sensor offsets, washouts, rathole sections, data acquired inside the casing). There are a number of techniques which could be used to patch the missing log data. These include linear regressions, multi-linear regressions (MLR), and the neural net approach. Linear regressions work well if there is a simple linear relationship between the two variables. MLR utilize more than one log data curves to produce a synthetic output log curve. **Figure 8(a)** and **Figure 8(b)** show an example where gamma ray, deep resistivity and neutron porosity curves have been used to generate synthetic bulk density log. When compared with the actual density log data (**Figure 8(a)**), the two curves (synthetic versus actual) match very well. The base line in the residuals in **Figure 8(c)** correspond to the middle of the synthetic curve. The difference between the measured log and the synthetic log is shown as a scatter in **Figure 8(c)**. Ideally, the scatter should be as minimal as possible with a consistent spread above and below the base line. The magnitude of the residuals therefore shows if the two logs are close enough or if there is systematic shift in the two log curves. If the synthetic log is systematically off, then the difference between the peaks and troughs of the two logs will be higher on one side than the other. This would shift the residuals above or below the base (zero) line. A neural net approach could be used if both linear and MLR approaches fail to generate a good synthetic log. This approach uses "Self Organizing Maps" (SOM) in order to allocate a node to each cluster of data points in the 3D space. MLP (multi-layer perception) is the basis of neural net. An example where neural net approach might help is to make permeability prediction from a set of input logs when there is a no good correlation between core porosity and core permeability.

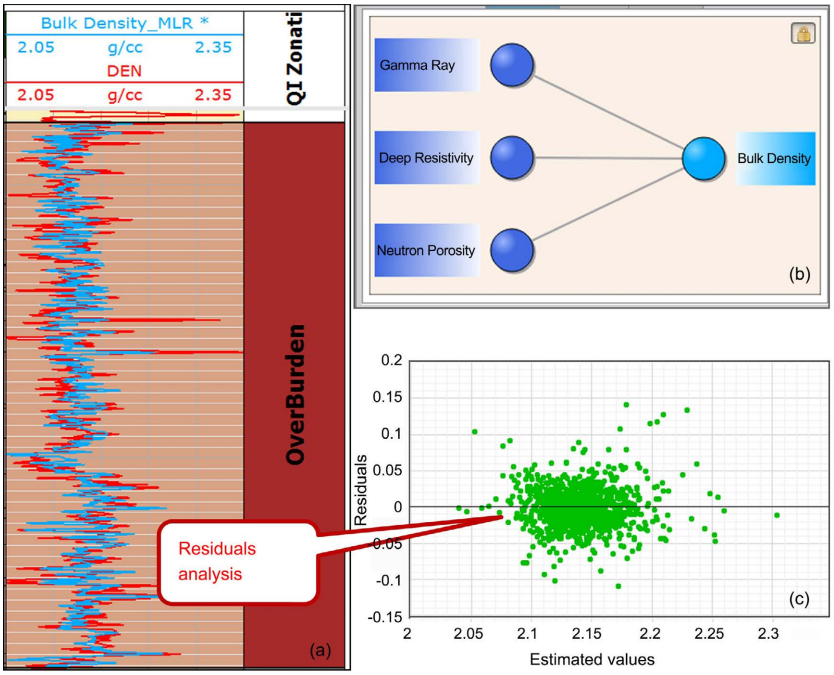

Figure 8. (a) Comparison of the actual and synthetic density logs using MLR approach; (b) Gamma ray, deep resistivity and neutron porosity curves have been used as input into MLR; (c) Residuals to compute the difference between the measured log and synthetic log. Residuals concentric around zero line (y-axis) and their small magnitude demonstrate a good match between the synthetic and actual logs.

2.2. Step-2: Identify Overburden and Reservoir Sections, and Fluid Fill

From the workflow shown in Figure 1, the crucial step post log data QC is for the logs to be able to distinguish between the overburden section and reservoir interval. This check is prudent before building a rock physics model and to have confidence on the validity and usefulness of the synthetic seismograms. If the logs are of good quality but are unable to distinguish between the different formations and the reservoir section, it would then make it difficult for the actual seismic to identify the different formations and reservoir section. Figure 9 shows a cross plot of V_p (x-axis) and V_s (y-axis). The overburden formations fall in distinct areas as shown in grey and orange colors. The reservoir section is located higher up on the crossplot in light green color. This distinction provides confidence on the seismic data to be able to identify reservoir interval from the overburden. At times, there could be further constraints which would pose limitations on what seismic can see. For instance, if the thickness of the reservoir is within the tuning thickness of seismic or if the reservoir is thinly bedded, this may make it difficult for the seismic to identify sands and different reservoir units.

In addition to identifying overburden and reservoir intervals, it is also critical that the density and sonic logs must respond to fluid changes within the reservoir interval. For this, one can use a cross plot between V_p (y-axis) and V_s (x-axis) within the reservoir section and color code with saturation curve. This is shown in Figure 10(a). The circled data points correspond to lower water saturations.

These data points belong to the thin oil rim shown by the circle in Figure 10(b). Shear velocities do not respond in fluids whereas compressional velocities become slower in lighter fluids. This makes the datapoints for the oil-bearing zone to shift left of the cross plot. Again, this gives confidence that the seismic data is likely to respond to fluid changes at the well location and potentially across the field. One should bear in mind that in reservoirs with relatively heavy oil where oil densities become closer to the density of the formation water, there might only be subtle or no effect on the density log and compressional log responses across the oil and water zones. In such circumstances, the cross plot in Figure 10(a) might not show any distinction across the two reservoirs.

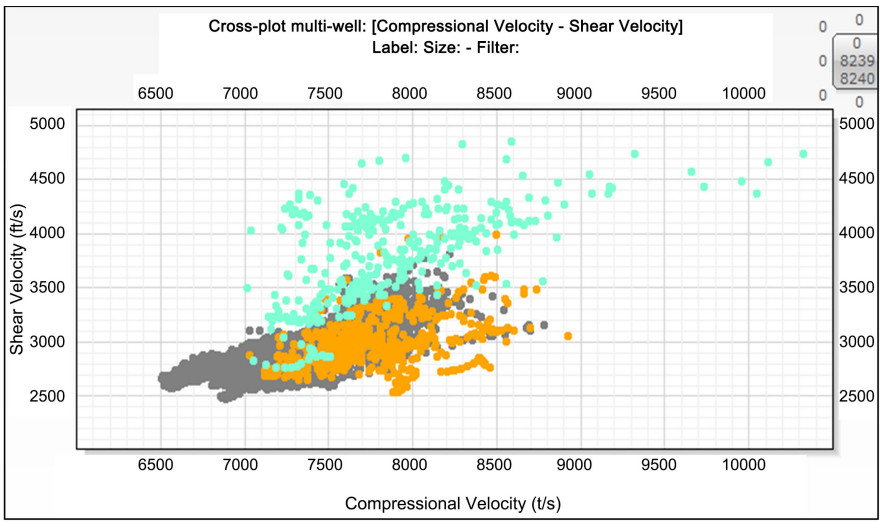

Figure 9. Crossplot of V_p and V_s to identify overburden and reservoir sections.

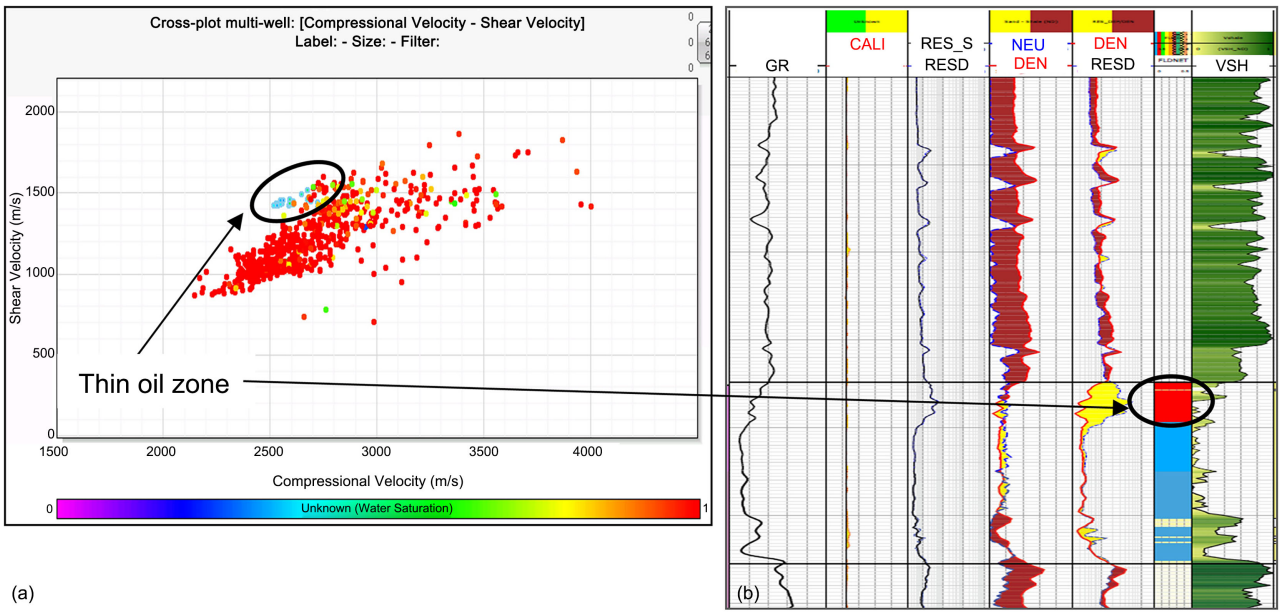

Figure 10. (a) Crossplot between compressional velocity and shear velocity (y-axis) color coded with saturations; (b) Log plot showing shale volume from neutron and density logs (track 1 from right), fluid flag (track 2), sonic-resistivity logs (track 3), neutron-density logs (track 4), and GR log (track 5).

The effect of fluid change is significantly pronounced when one looks at the bulk moduli of rocks and fluids (notably incompressibility and rigidity of the rock) as opposed to V_p and V_s logs. The two properties are computed using Equations (1) and (2) below.

$$\lambda_{\_\text{rho}} = \text{Incompressibility of the rock} = \text{Ip}^2 - 2\text{Is}^2 \quad (1)$$

$$\mu_{\_\text{rho}} = \text{Rigidity of the rock} = \text{Is}^2 \quad (2)$$

$\lambda_{\_\text{rho}}$ corresponds to incompressibility of the rock and $\mu_{\_\text{rho}}$ corresponds to rigidity (or resistance to deformation) of the rock. Ip and Is correspond to compressional and shear impedances of the rock respectively. The compressional and shear impedance are computed by multiplying compressional and shear velocities with the density of the formation (DEN*Vp and DEN*Vs). As shear impedance of the rock becomes high, it becomes denser and hence becomes more rigid to deformation.

A typical cross plot of the two rock properties ($\lambda_{\_\text{rho}}$, $\mu_{\_\text{rho}}$) is shown in **Figure 11**. The plot is color coded with saturations. $\lambda_{\_\text{rho}}$ (x-axis) moves towards higher values for less compressible rocks. In this particular example, as water saturation increases (green and blue points), the rock becomes less and less compressible (water is incompressible). Hence $\lambda_{\_\text{rho}}$ values increase. The data points color coded in red and yellow belong to a gas bearing zone where $\lambda_{\_\text{rho}}$ shows lower values. $\mu_{\_\text{rho}}$ is plotted on the y-axis and which corresponds to rigidity or shear impedance of the rock. The fact that shear velocities are independent of fluids, the change in fluid saturations have a higher impact on x-axis as opposed to y-axis. Note that the spread in data points on the y-axis is due to the rock response itself (and not due to fluids) as a result of a change in shear impedance of the rock.

The two rock property parameters can also be used to distinguish between the hydrocarbon bearing sands and shale intervals within the reservoir section. **Figure 12(a)** shows a crossplot where oil bearing sands and reservoir shales (highlighted in brown and black respectively) are clearly identifiable on the cross plot. The reservoir sands are highlighted in "yellow" from the neutron-density separation in **Figure 12(b)** (track 1 from right).

2.3. Step-3: Computation of Petrophysical Parameters for Rock Physics Model

In previous sections, the QC'd log data and rock property parameters have shown to be able to identify between the overburden and reservoir sands, and the fluid fill inside the reservoir. The next step in building a rock physics model is the determination of petrophysical parameters which subsequently feed into the Gassmann equations to compute V_p_syn and V_s_syn.

For a typical rock physics model, one would need to know the petrophysical parameters given in the following equations [20] [21]. The description of the various acronyms is given in the Nomenclature of this paper.

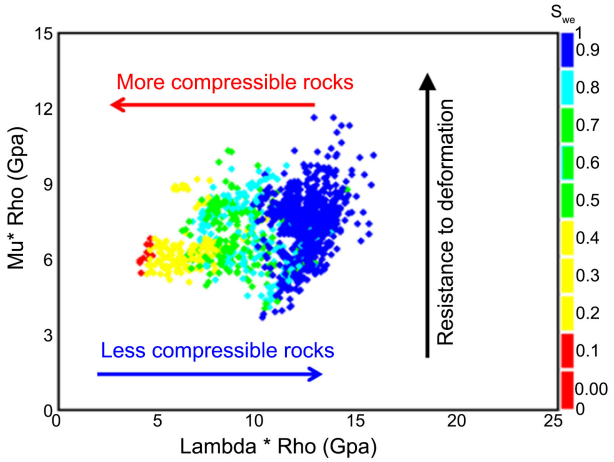

Figure 11. Crossplot between the Incompressibility (λ_{rho}) and Rigidity (μ_{rho}) of the rock.

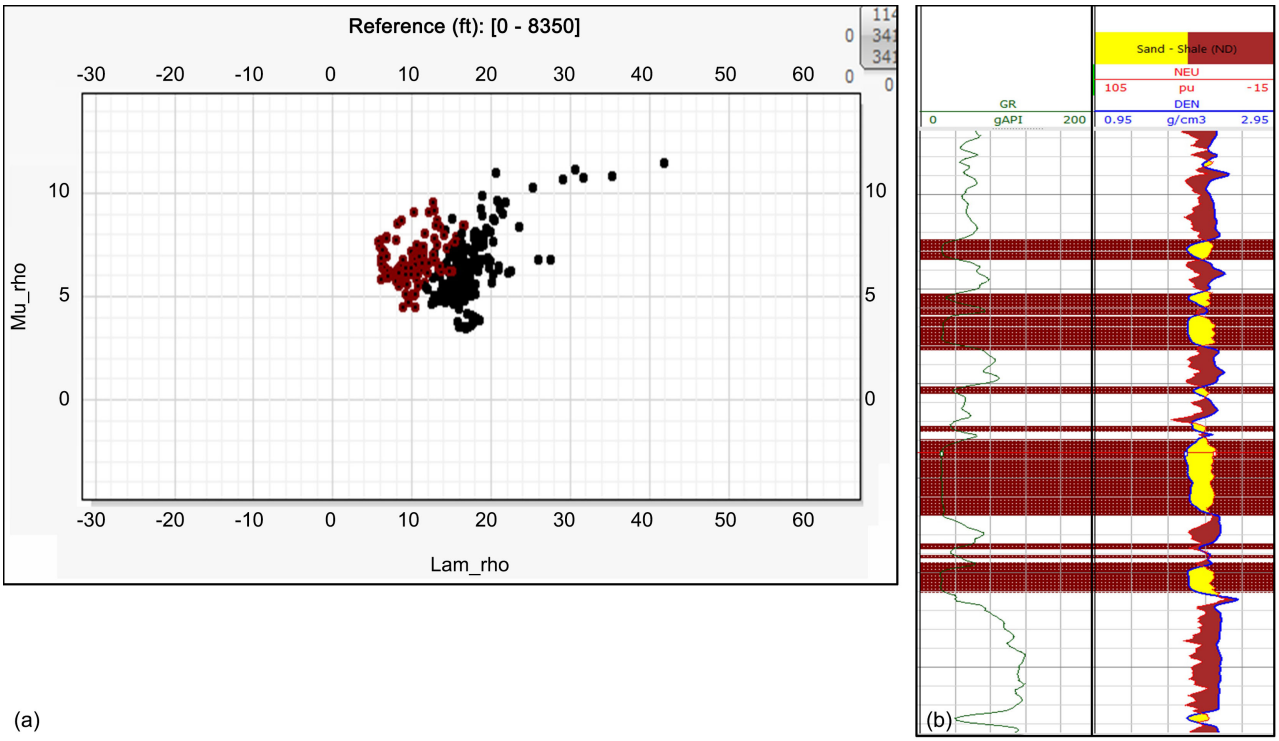

Figure 12. (a) Crossplot between λ_{rho} and μ_{rho}. (b) Log plot showing neutron and density logs (track 1 from right), and GR (track 2).

$$Bvw = SwT * PhiT \tag{3}$$

$$Vbw = PhiT - Phie \tag{4}$$

$$Vw = Swe * Phie = Bvw - Vbw \tag{5}$$

$$Vhc = (1 - Swe) * Phie = Phie - Vw \tag{6}$$

$$Vclay = Vshale - Vbw \tag{7}$$

$$Vsand = (1 - Vshale - Phie) = (I - Vclay - PhiT) \tag{8}$$

For QC purposes, remember

$$\text{PhiT} = \text{Vbw} + \text{Vw} + \text{Vhc} \tag{9}$$

$$\text{Phie} = \text{Vw} + \text{Vhc} \tag{10}$$

$$\text{Vsand} + \text{Vclay} + \text{PhiT} = 1 \tag{11}$$

$$\text{Vsand} + \text{Vshale} + \text{Phie} = 1 \tag{12}$$

In case of multimineral approach (combining Equations (9) and (11), and assuming three minerals)

$$\text{Vmin1} + \text{Vmin2} + \text{Vmin3} + \text{Vbw} + \text{Vw} + \text{Vhc} = 1 \tag{13}$$

The computation of the effective porosity (Phie) is a key to solve the various petrophysical parameters given in Equations (3)-(8) [20]. For this, one can use NMR log data, core data, or the modules available in various petrophysical software.

There is another technique which could help compute volume of dry clay (Vclay) and which in turn helps to solve Equations (3)-(8). For instance, if Vclay is known, one can then compute Vbw (Vclay+Vsh). From this, one can compute Vw (Bvw-Vbw, where Bvw is known from Archie saturation). Then, the effective porosity and the rest of the petrophysical parameters can be computed. The technique for resolving Vclay is shown in Equations (14)-(16). Apparently, Vclay can be related to the density and neutron log responses of the formation. The underlying principle in the computation relies in the difference between the density and neutron porosities which is purely the effect of additional hydrogen present in the clays (this is the hydrogen in the clay elements instead of hydrogen in pore fluids). In the absence of clays (that is matrix only), there will be no hydrogen atoms, and hence no difference between the two porosities (for pure clay, density porosity = 0 and Neutron porosity is equal to the hydrocarbon index (HI) of the dry clay).

$$V_{\text{cl(dry)}} = \frac{\varphi_N - \varphi_d}{\text{HI}_{\text{cl(dry)}}} \tag{14}$$

$$\text{HI} = \frac{\text{Amount of hydrogen in sample}}{\text{Amount of hydrogen in pure water at STP}} \tag{15}$$

$$\text{HI} = \frac{\rho_m \cdot N_H / M}{0.111} \tag{16}$$

For Equation (16) to work, it is better if clay is dominated by a single mineral or if there is known split between more than one clay minerals.

2.4. Step-4: Building a Rock Physics Model—Fluid Substitution

Gassmann equations are by far the most widely used relations to calculate seismic velocity changes because of different fluid saturations in reservoirs. The bulk moduli along with shale volume, porosity and saturation information (the parameters computed in the previous section) are used as input into the Gassmann equations [14] [15].

$$\frac{\kappa_{sat}}{\kappa_0 - \kappa_{sat}} = \frac{\kappa_{dry}}{\kappa_0 - \kappa_{dry}} + \frac{\kappa_{fl}}{\phi\left(\kappa_0 - \kappa_{fl}\right)} \tag{17}$$

Bulk Modulus of the saturated rock

Bulk Modulus of the frame

Bulk Modulus of fluid inside the pores

Bulk modulus is the ratio of applied differential pressure to volumetric strain (bulk volume deformation). Therefore, bulk modulus essentially corresponds to volumetric change as a result of hydrostatic stress (both rocks and fluids respond to it). This essentially corresponds to stiffness of the rock. One might wonder why we use bulk moduli in the Gassmann equations as opposed to V_p, V_s and DEN logs. The differential pressure inside the reservoir (confining pressure minus pore pressure) changes as one enters from non-reservoir into a reservoir interval. The change in compressional and shear wave velocities, as a result of a change in differential pressure, is little when compared with a change in the bulk moduli.

Shear sonic is a pre-requisite for Gassmann substitution. If unavailable, one can compute using dry rock Poisson's ratio, locally derived V_P-V_s trends and P-modulus method. The details of these methods is outside the scope of this paper. The first two methods assume that shear data is available in neighboring or analogue wells.

Rewriting Gassmann Equation (17) helps compute synthetic V_p and V_s curves.

$$V_p = \sqrt{\frac{K_{bulk} + \frac{4}{3}\mu_{bulk}}{\rho_b}} \tag{18}$$

$$V_s = \sqrt{\frac{\mu_{bulk}}{\rho_b}} \tag{19}$$

Figure 13 shows an example where synthetic logs from Gassmann equation were successfully compared with LWD and wireline logs. The first track (from left) is a lithology track acquired from the mud logs and core data. The second track shows hydrocarbon bearing sands (in RED) from the log derived POR and BVW saturations. The next three tracks show bulk density, and compressional and shear velocities. Both wireline and LWD logs were acquired in this well for sonic compressional, shear and bulk density of the formation. Rock physics model was built using this log data to generate synthetic bulk density, and compressional and shear velocities. The synthetic (modelled) logs are compared with both wireline and LWD log data. The wireline logs are shown in Green, LWD logs are shown in Black, and the predicted logs from Gassmann equation are shown in Red. All three show a very good match. The last three tracks show a comparison of μ_{rho} (in Red) and λ_{rho}, (in Blue) for wireline, LWD and model loges. Again, all of them show a very good match to identify the hydrocarbon bearing sands in the reservoir.

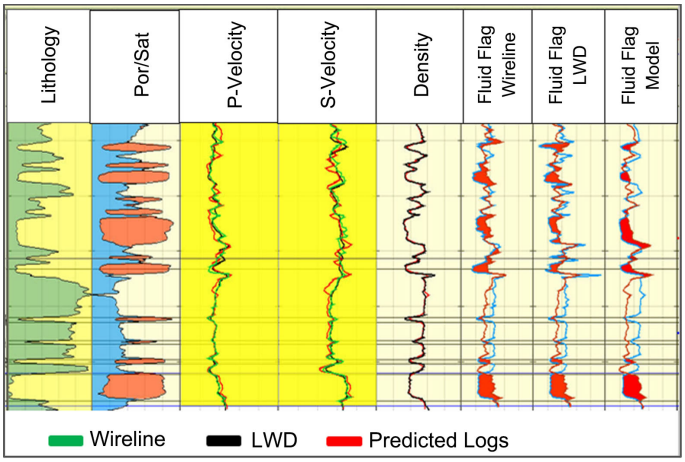

Figure 13. Log plot showing the wireline and LWD log data for bulk density, and compressional and shear velocities (tracks 4 - 6 from right) and their comparison with synthetic logs (shown in Red) computed from Gassmann equations.

Once the rock physics model has shown promising results to identify reservoir interval, and hydrocarbon bearing sands, seismic data can then be converted into rock properties ($\lambda_{\_rho}$ and $\mu_{\_rho}$) at the well locations. **Figures 14(a)-(c)** show a cross plot between $\lambda_{\_rho}$ (x-axis) and $\mu_{\_rho}$ (y-axis) using the wireline, LWD and model logs respectively. **Figure 14(d)** shows a similar cross plot with the two rock properties derived from the seismic data. The seismic derived rock properties are in good agreement with those from wireline and model logs. Once one has built enough confidence that seismic data is responding to changes in the reservoir fluid saturation at well locations, it should be feasible to invert seismic for the reservoir properties (Vsh, Sw, Porosity) away from the wells.

In previous sections, the conditioned log data along with rock property parameters and Gassmann substituted synthetic curves have shown to be able to distinguish between the overburden and reservoir sections and respond to fluid changes inside the reservoir sands. This builds sufficient confidence in the robustness of the rock physics model. The final step in the rock physics model is to generate a synthetic seismogram and compare with the actual seismic trace at the well location. **Figure 15** shows synthetic seismogram (track 1 from right) generated from the QC'd log data mentioned earlier in the paper. The actual seismic trace is shown in track 2 from right. Both synthetic and seismic traces match very well at the well location. This completes the QI feasibility study. Additional analysis of the seismic data can be done as part of QI attributes study by utilizing DHI and AVO responses. This can further support the QI feasibility work. A subsequent seismic inversion work (deterministic or probabilistic) could also be carried out to understand the distribution of reservoir properties in the field/area. However, both QI attributes study and seismic inversion work are outside the scope of this paper.

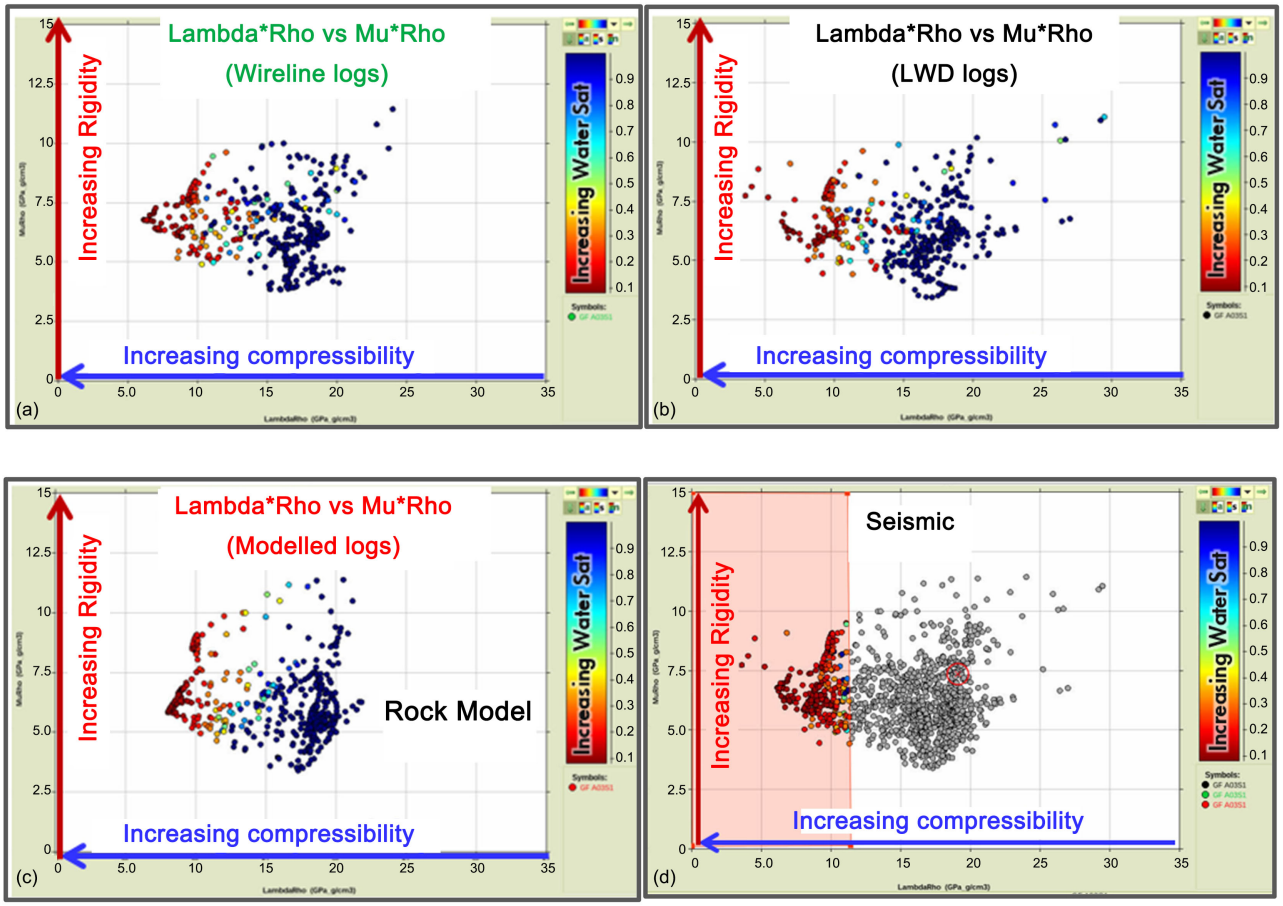

Figure 14. (a)-(c) show a crossplot between λ_{rho} and μ_{rho} using the wireline, LWD and model log data respectively. (d) shows a similar crossplot with rock properties derived from the seismic data.

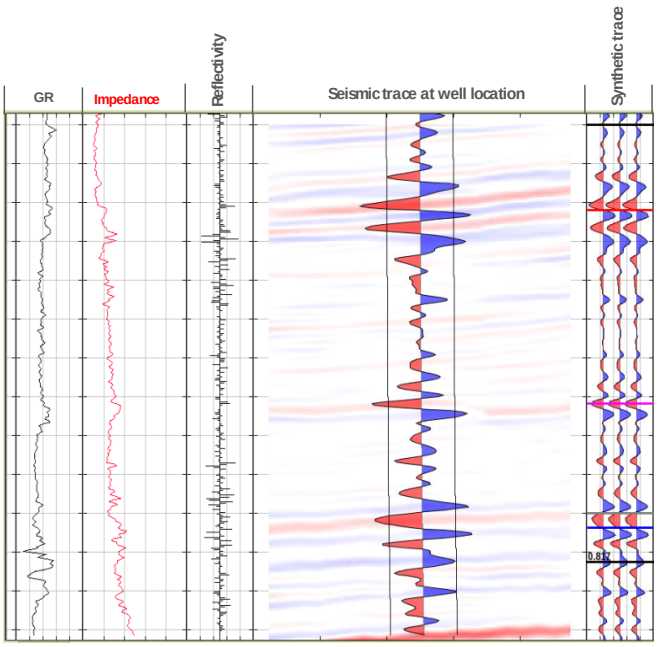

Figure 15. Comparison between the synthetic seismogram (track 1 from right) and the seismic trace (track 2 from right) at a well location.

3. Conclusions

The main conclusions from this work are summarised as follows.

- This paper provides a simplified step by step approach for building a rock physics model.
- A poor-quality rock physics model may lead to significant financial and HSSE implications by drilling wells in undesired locations. The work presented highlights the importance of an exhaustive log data QA/QC which forms the basis of building a good quality rock physics model.
- The paper shows that a few key cross plots and rock property parameters are adequate in distinguishing the overburden and reservoir sections, and to help identify fluids within the reservoirs.
- In the case study presented, both compressional and shear velocities can potentially distinguish between the overburden and reservoir sections. It is also shown that rock property parameters including λ_{rho} (incompressibility of the rock) and μ_{rho} (rigidity of the rock) provide another powerful means of identifying fluid changes inside the reservoirs.
- Seismic data provides the only source for scanning across the entire field including OB sections. QI feasibility work, QI attributes work, DHI and AVO responses, and seismic inversion work provides powerful insights into the reservoir and field development plans.
- In the case study presented, the robustness of the simplified rock physics model has helped seismic data to successfully distinguish hydrocarbon bearing reservoir sands from non-reservoir shales.

Conflicts of Interest

The authors declare no conflicts of interest regarding the publication of this paper.

References

[1] Hamilton, E.L. and Bachman R.T. (1982) Sound Velocity and Related Properties of Marine Sediments. *The Journal of the Acoustical Society of America*, **72**, 1891-1904. https://doi.org/10.1121/1.388539

[2] Krief, M., Garat, J., Stellingwerff, J. and Ventre, J. (1990) A Petrophysical Interpretation Using the Velocities of P and S Waves (Full-Waveform Sonic). *The Log Analyst*, **31**, 355-369.

[3] Dai, J., Snyder, F. and Dutta, N. (2002) Detection and Estimation of Gas Hydrates Using Rock Physics and Seismic Inversion: Examples from the Northern Deepwater Gulf of Mexico. *The Leading Edge*, **23**, 60-66. https://doi.org/10.1190/1.1645456

[4] Domenico, S.N. (1974) Effect of Water Saturation on Seismic Reflectivity of Sand Reservoirs Encased in Shale. *Geophysics*, **39**, 759-769. https://doi.org/10.1190/1.1440464

[5] Castagna, J.P., Batzle, M.L. and Eastwood, R.L. (1985) Relationships between Compressional-Wave and Shear-Wave Velocities in Clastic Silicate Rocks. *Geophysics*, **50**, 571-581. https://doi.org/10.1190/1.1441933

[6] Greenberg, M.L. and Castagna, J.P. (1992) Shear Wave Velocity Estimation in Po-

rous Rocks: Theoretical Formulation, Preliminary Verification and Applications. *Geophysical Prospecting*, **40**, 159-209. https://doi.org/10.1111/j.1365-2478.1992.tb00371.x

[7] Gardner, G.H.F., Gardner, L.W. and Gregory, A.R. (1974) Formation Velocity and Density—The Diagnostic Basics for Stratigraphic Traps. *Geophysics*, **39**, 770-780. https://doi.org/10.1190/1.1440465

[8] Faust, L.Y. (1951) A Velocity Function Including Lithologic Variation. *Geophysics*, **18**, 271-288. https://doi.org/10.1190/1.1437869

[9] Rudman, A.J., Whaley, J.F., Blakely, R.F. and Biggs, M.E. (1975) Transform of Resistivity to Pseudo-Velocity Logs. *AAPG Bulletin*, **59**, 1151-1165. https://doi.org/10.1306/83D91F47-16C7-11D7-8645000102C1865D

[10] Adcock, S. (1993) In Search of the Well-Tie: What If I Don't Have a Sonic Log? *The Leading Edge*, **12**, 1161-1164. https://doi.org/10.1190/1.1436929

[11] Zoeppritz, K. and Erdbebenwellen, V.B. (1919) On the Reflection and Propagation of Seismic Waves. *Gottinger Nachrichten*, **1**, 66-84.

[12] Aki, K. and Richards, P.G. (1980) Quantitative Seismology: Theory and Methods. W. H. Freeman and Company, San Francisco.

[13] Shuey, R.T. (1985) A Simplification of the Zoeppritz Equations. *Geophysics*, **50**, 609-614. https://doi.org/10.1190/1.1441936

[14] Gassmann, F. (1951) Elastic Waves through a Packing of Spheres. *Geophysics*, **16**, 673-685. https://doi.org/10.1190/1.1437718

[15] Geertsma, J. and Smit, D.C. (1961) Some Aspects of Elastic Wave Propagation in Fluid Saturated Porous Solids. *Geophysics*, **26**, 169-181. https://doi.org/10.1190/1.1438855

[16] Dvorkin, J., Gutierrez, M.A. and Grana, D. (2014) Seismic Reflections of Rock Properties. Cambridge University Press, Cambridge. https://doi.org/10.1017/CBO9780511843655

[17] Bosch, M., Muckerji, T. and Gonzalez, E.F. (2010) Seismic Inversion for Reservoir Properties Combining Statistical Rock Physics and Geostatistics: A Review. *Geophysics*, **75**, 165-176. https://doi.org/10.1190/1.3478209

[18] Kittridge, M.G., Braunsdorf, N.R. and Bryndzia, L.T. (2008) Seismic Petrophysics—Integration to Enable Geologically-Sensible Rock Physics: A Gulf of Mexico Demonstration. *Society of Petrophysicists and Well-Log Analysts* 49*th Annual Logging Symposium*, Austin, TX, 25-28 May 2008, SPWLA-2008-RRR.

[19] Avseth, P., Mukerji, T. and Mavko, G. (2010) Quantitative Seismic Interpretation. Cambridge University Press, Cambridge.

[20] Truman R. B., Howard W. E., Luffel D. L. (1989) Shale Porosity—Its Impact on Well Log Modelling and Interpretation. SPWLA 30th Annual Logging Symposium, Denver, Colorado, 11-14 June 1989, SPWLA-1989-Q.

[21] Luffel, D.L. and Guidry, F.K. (1989) Reservoir Rock Properties of Devonian Shale from Core and Log Analysis. *The Society of Core Analysts Conference*, Vol. I, Paper 8910.

Nomenclature

Bvw = total water fraction of the pore volume
DEN = formation bulk density
DEN_syn = synthetic bulk density
DRHO = density correction log
DT = sonic transit time
$HI_{cl(dry)}$ = hydrogen Index of clay in the rock
Ip = compressional impedance of the rock
Is = shear impedance of the rock
Kbulk = Ksat = saturated rock bulk modulus
Kdry = effective bulk modulus of the dry rock, sometimes called Kmatrix
Kfl = pore fluid bulk modulus
K0 = effective bulk modulus of the minerals making up of the matrix
M = molecular weight of clay
N_H = number of hydrogen in the molecule of clay
PEF = photoelectric factor log
Phie = effective porosity
PhiT = total porosity
QA = quality assurance
QC = quality checking
Rho_m = density of clay
Swe = effective water saturation
SwT = total water saturation
Vbw = clay bound water fraction of the pore volume
Vclay = volume of dry clay
Vhc = hydrocarbon volume fraction of the pore volume
Vp = compressional velocity
Vp_syn = synthetic compressional velocity
Vs = shear velocity
Vs_syn = synthetic shear velocity
Vsand = volume of sand
Vshale = volume of shale
Vw = mobile water fraction of the pore volume
Ubulk = Usat = Udry = effective shear modulus
λ_{rho} = incompressibility of the rock
μ_{rho} = rigidity (or resistance to deformation) of the rock